



THE UNIVERSITY *of* EDINBURGH

Edinburgh Research Explorer

## Icosahedral (H<sub>2</sub>)<sub>13</sub> supermolecule

**Citation for published version:**

Ackland, G & Martinez-Canales, M 2018, 'Icosahedral (H<sub>2</sub>)<sub>13</sub> supermolecule' *Physical Review Materials*, vol. 2, no. 9.

**Link:**

[Link to publication record in Edinburgh Research Explorer](#)

**Document Version:**

Peer reviewed version

**Published In:**

*Physical Review Materials*

**General rights**

Copyright for the publications made accessible via the Edinburgh Research Explorer is retained by the author(s) and / or other copyright owners and it is a condition of accessing these publications that users recognise and abide by the legal requirements associated with these rights.

**Take down policy**

The University of Edinburgh has made every reasonable effort to ensure that Edinburgh Research Explorer content complies with UK legislation. If you believe that the public display of this file breaches copyright please contact [openaccess@ed.ac.uk](mailto:openaccess@ed.ac.uk) providing details, and we will remove access to the work immediately and investigate your claim.



# The Icosahedral $(\text{H}_2)_{13}$ Supermolecule

Graeme J. Ackland,<sup>1</sup> Jack Binns,<sup>2</sup> Ross Howie,<sup>2</sup> and Miguel Martinez-Canales<sup>1</sup>

<sup>1</sup>*CSEC, School of Physics and Astronomy, The University of Edinburgh, Edinburgh EH9 3FD, UK*

<sup>2</sup>*Center for High Pressure Science Technology Advanced Research (HPSTAR), Shanghai, China.*

(Dated: August 2, 2018)

We investigate a range of possible materials containing the supermolecular form of hydrogen comprising 13  $\text{H}_2$  molecules arranged in an icosahedral arrangement. This supermolecule consists of freely rotating 12  $\text{H}_2$  molecules in an icosahedral arrangement, enclosing another freely rotating  $\text{H}_2$  molecule. To date, this supermolecule has only been observed in a compound with Iodane (HI). The extremely high hydrogen content suggests possible application in hydrogen storage so we examine the possibility of supermolecule formation at ambient pressures. We show that *ab initio* molecular dynamics calculations give a good description of the known properties of the  $\text{HI}(\text{H}_2)_{13}$  material, and make predictions of the existence of related compounds  $\text{Xe}(\text{H}_2)_{13}$ ,  $\text{HBr}(\text{H}_2)_{13}$  and  $\text{HCl}(\text{H}_2)_{13}$ , including a symmetry-breaking phase transition at low temperature. The icosahedral  $(\text{H}_2)_{13}$  supermolecule, remains stable in all these compounds. This suggests  $(\text{H}_2)_{13}$  is a widespread feature in hydrogen compounds, and that appropriately-sized cavities could hold hydrogen supermolecules even at low pressure. The structure of the supermolecule network is shown to be independent of the compound at equivalent density.

PACS numbers:

## I. INTRODUCTION

Hydrogen-rich compounds have attracted a lot of attention because of their potential applications for fuel cell storage<sup>1</sup> and for high- $T_c$  superconductors<sup>2</sup>. In particular, high pressure has been an effective thermodynamic variable in the synthesis of such compounds exemplified by recent experimental and theoretical breakthroughs.<sup>1-15</sup>

The developments in high-pressure diamond anvil cells have pushed the frontiers, with pressures up to 200 GPa now obtained routinely for most materials. However experimental studies involving hydrogen prove both problematic and costly, through the premature failure of the anvils due to hydrogen diffusion and embrittlement. Computational structure searches based on density functional theory have now assumed an important role as a screening method in finding materials of potential interest as targets for synthesis<sup>16,17</sup>, and first suggested very large hydrogen fraction compounds as a route to high- $T_c$  superconductivity or energy storage<sup>18</sup>

Recently, Binns *et al.* synthesized<sup>14</sup>  $\text{HIH}(\text{H}_2)_{13}$ , a compound with a number of remarkable features. At over 96% stoichiometric ratio, it has the highest known molecular hydrogen content of any compound. While this stoichiometry suggests  $\text{IH}_{27}$  to be a solid solution, X-ray diffraction shows a primitive cubic lattice of iodine atoms<sup>14</sup>. The material can be regarded as a 1:1 stoichiometric compound comprising iodane molecules and so-called  $(\text{H}_2)_{13}$  supermolecules. Assuming that each  $\text{H}_2$  is spherical, as is the case for phase I of solid Hydrogen, three obvious possibilities present themselves for the supermolecule: cuboctahedron, icosahedron or dynamically spherical. Icosahedral symmetry would be curious, because the fivefold symmetry is incompatible with the cubic structure. The structure suggested by simulation has a doubled unit cell along  $\{111\}$ , with two icosahedral su-

per molecules in opposite orientations: this more complex structure is fully compatible with existing experimental X-ray (which cannot detect the hydrogen positions), and Raman experimental data.

Hydrogen-storage materials face an intrinsic trade-off between strongly binding hydrogen (atomic or molecular) for stability and the energy required to release  $\text{H}_2$  for applications. The  $(\text{H}_2)_{13}$  units are especially attractive because they store a large amount of hydrogen in a weakly bound molecular form. Other hydrogen-rich materials such as methane hydrates or ammonium borohydride require energy to break strong bonds between the hydrogen and other elements<sup>1,19</sup>.

It is interesting to consider whether the supermolecules may be recovered to ambient conditions in any material.  $\text{HI}(\text{H}_2)_{13}$  decomposes on depressurization, but this may be because the HI molecule itself is unstable to decomposition to  $\text{H}_2$  and  $\text{I}_2$  at ambient conditions<sup>20</sup>. Since the nature of the binding in this material remains unknown, it is unclear whether this lack of recoverability is a necessary consequence of the bonding type, or if other similar materials might be recoverable. Replacing the iodane molecule with something stable is an obvious first step, e.g. other hydrogen halides, large metallic atoms, noble gases or small polar molecules like chloromethane.

Here, we show that density functional theory (DFT) and *ab initio* molecular dynamics (AIMD) produce an accurate description of the known  $\text{HI}(\text{H}_2)_{13}$  compound and analysis its behaviour under depressurization. Using these results, we investigate other potential compounds that could exhibit this hydrogen supermolecules and find  $\text{HBr}(\text{H}_2)_{13}$ ,  $\text{HCl}(\text{H}_2)_{13}$  and  $\text{Xe}(\text{H}_2)_{13}$  to all be dynamically stable. The unprecedented stability of these compounds suggests that  $(\text{H}_2)_{13}$  may be exhibited in a variety of systems and if recoverable, could have potential interest in hydrogen storage applications.

## II. METHODS

DFT calculations were performed using the CASTEP planewave pseudopotential package<sup>21</sup>, using norm-conserving pseudopotentials, a minimum of  $2 \times 2 \times 2$  k-points and an energy cutoff of 1200 eV. Temperature and anharmonic effects were accounted for by performing Born-Oppenheimer AIMD, using a 0.5 fs timestep. AIMD runs were typically 3 ps long. This is necessarily far too short of experimental timescales, but much longer than any characteristic oscillation in the system, such that any soft-phonon or martensitic transition could easily occur. It is also long enough to observe the free rotation of H<sub>2</sub> molecules. We used a  $2 \times 2 \times 2$  supercell with eight supermolecular units (224 atoms).

In all cases, the heavy molecules form a time-averaged structure close to simple cubic, so for ease of comparison throughout, we always report the lattice parameter associated with this lattice. This is also the only structural variable that can be determined from X-ray diffraction because the H<sub>2</sub> molecules are essentially invisible to X-rays.

The choice of exchange correlation functional is a highly debated topic in DFT studies of hydrogen. In a benchmarking studies on hydrogen the BLYP functional<sup>22,23</sup> was shown to give results closest to Quantum Monte Carlo calculations<sup>24,25</sup>, for transition pressures and vibrational frequencies, due mainly to the correct asymptotic behaviour at high charge density gradient<sup>26</sup>.

Van der Waals interactions are not well accounted for in traditional semilocal exchange-correlation functionals. These, however, could be important holding the hydrogen molecules together. It has been shown that explicit nonlocal treatment of the van der Waals interaction is of secondary importance for hydrogen at pressures beyond 200 GPa<sup>26</sup>. The calculations shown here are performed with BLYP unless otherwise stated, with other exchange-correlation functionals<sup>27–30</sup> used for comparison in some configurations (Figure 1). As expected, we find Tkatchenko–Scheffler van der Waals corrections produce no significant differences over the other semilocal functionals. The radial distribution function (RDF) shown in Fig. 1 shows that, at a given volume, the structural details are effectively independent of functional. There is a bigger discrepancy in the computed DFT pressure. BLYP gives by far the largest values, and consequently a much higher “pressure” at given density compared with other functionals or with experiment. Pressure is a derived quantity in DFT, whereas volume is directly input, so it is reasonable to compare calculations at the same density.

In AIMD at 300 K, we observe that the hydrogen forms well defined molecules with a high-frequency, Raman-active stretching mode (vibron). Molecules behave as mildly-inhibited rotors, so we expect their Raman signature to be that of a quantum rotor (roton) at low pressure, and a rotating harmonic oscillator (libron) at higher

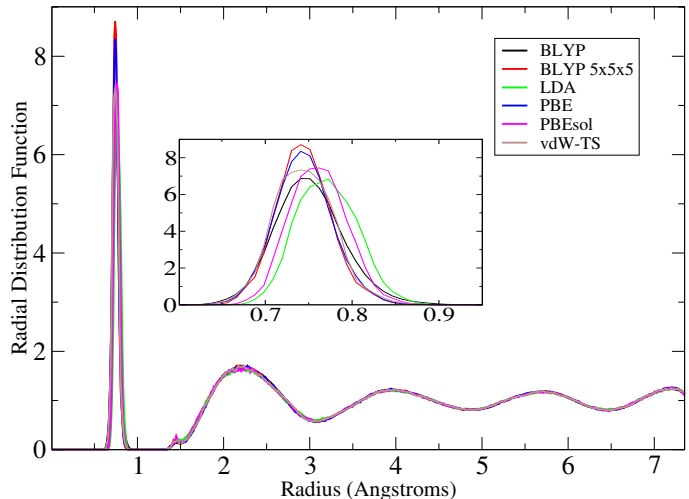


FIG. 1: All-atom RDF in HBr(H<sub>2</sub>)<sub>13</sub> at lattice parameter 5.25 Å, calculated with a variety of exchange-correlation functionals. The small feature at 1.5 Å is the HBr bond. The calculated pressures are 16.7 GPa (BLYP,<sup>22,23</sup> 5<sup>3</sup> k-point grid), 20.5 GPa (BLYP,<sup>22,23</sup> 16.4 GPa (PBE<sup>27</sup>), 11.3 GPa (LDA<sup>29</sup>), 13.3 GPa (PBEsol<sup>28</sup>) and 15.3 GPa (PBE+TS<sup>30</sup>). (*inset*) Detail for the first peak, showing that LDA and PBEsol give noticeably longer bondlengths commensurate with their lower pressures. MD simulations are NVT at 300 K, equilibrated for 1ps, then averaged over 1.5ps and contain eight supermolecules.

pressures. This also means that the molecules exhibit the correct spherical symmetry and that, over time, the indistinguishability of the two nuclei is respected. It is not clear to what extent the single molecule angular momentum  $J$  is a good quantum number, but in any case fully quantum treatment with ortho- and para-hydrogen is not currently possible. Below 100K, molecular rotation stops, orientations are frozen into a rotational glass.

Quantum nuclear effects are neglected in classical MD, and there are several distinct places to consider where this can be problematic<sup>31</sup>.

- The high frequency H<sub>2</sub> molecular vibration is thermally excited in classical MD, but essentially not in the quantum case. It adds a spurious contribution to the heat capacity which is therefore not reliable, and a zero-point energy contribution to the total energy. However, these contributions are essentially the same in all structures, and so cancel out in the free energy differences which determine stability.
- The volume-dependence of the zero-point motion makes a contribution to the pressure. This is significant at pressures above 200 GPa where the H<sub>2</sub> vibron weakens significantly<sup>31</sup>. At lower pressures, it is of order 1 GPa, close to the uncertainty due to exchange-correlation functional.
- The zero-point motion means that there is already

some energy in the bond, so breaking it would be easier if quantum nuclear effects were considered. However, in our simulations we do not see significant bond breaking.

- Non-interacting hydrogen molecules behave as quantum rotors with energy  $\hbar^2 J(J+1)/2I$ , where  $I$  is the moment of inertia. The first excited state has energy around 170 K ( $\text{H}_2$ ) or 85 K (other molecules), so the thermal excitation implied by our 300 K classical simulations are reasonable. Furthermore, the classical free rotor behaviour is a good representation of the spherically-symmetric  $J = 0$  ground state. Thus we expect our supermolecule calculations to correctly describe the symmetry, just as classical MD of solid hydrogen gave an accurate qualitative prediction for the melting point of the “quantum rotor” phase<sup>32</sup>. By contrast, cooling simulations which show a symmetry-breaking phase transition are likely to overestimate the transition temperature.
- The requirement for antisymmetric wavefunctions means that the nuclear spin states of ortho- and para- hydrogen couple to even and odd  $J$  states respectively. This causes a slow equilibration of the roton energy. However, it only applies when  $J$  is a good quantum number. We monitor the angular momentum autocorrelation and find that typically the classical rotor cannot complete a full rotation without decorrelating. Thus the rotors are coupled,  $J$  is not a good quantum number, only the wavefunction of the entire system need be antisymmetric, and the nuclear spin state does not affect the dynamics.

So we expect any predictions of room temperature structures to be robust with regard to quantum nuclear effects

The DFT calculations give reliable indications of stability, but to obtain further insight one must look beyond the standard outputs to consider the nature of the bonding. Pure high pressure hydrogen changes under pressure from normal molecular phases, to phases in which the electron is squeezed out of the bond, making it weaker and longer<sup>6,7,33–38</sup>.

We have developed some techniques for imaging and analysing rotating molecules. All of these depend on being able to identify  $\text{H}_2$  molecules. To do this, we first identify the nearest neighbor of each iodine. Then, we find the nearest neighbour of each remaining hydrogen atom. Provided each atom is its neighbor’s neighbor, this uniquely defines molecules. This procedure works at all but a few timesteps at the highest pressures and temperatures considered here, when H-H bond reconstruction sometimes occurs. Such transforming configurations are excluded from the statistics.

Once molecules are identified, we can define a length  $r_k$  and angular momentum  $\mathbf{l}_k$  for each molecule  $k$ . For

the vibrons, we exploit the fact that Raman activity involves an in-phase symmetric stretch of all the molecules. We sum the total length of all molecules and build the velocity autocorrelation function

$$\text{VACF}(t) = \left\langle \frac{d}{dt} \sum_k r_k(t) - \frac{d}{dt} \sum_k r_k(0) \right\rangle$$

and the autocorrelation of the angular momentum:

$$\text{LACF}(t) = \left\langle \frac{d}{dt} \sum_k \mathbf{l}_k(t) - \frac{d}{dt} \sum_k \mathbf{l}_k(0) \right\rangle.$$

The peaks in the Fourier transform of VACF correspond to the Raman-active vibron modes<sup>35</sup>. where  $\mathbf{l}_k$  is the angular momentum of molecule  $k$  with respect to its centre of mass. Interpretation of the LACF is more subtle. If we had non-rotating molecules, its Fourier transform would give the librational mode frequencies. For free rotors the quantized energies are unrelated to the period of rotation and are simply  $J(J+1)\hbar^2/mr_k^2$ . In the rotor case, the LACF tells us for how long the molecule rotates unhindered.

#### A. The known material $\text{HI}(\text{H}_2)_{13}$

The only currently known material containing the  $(\text{H}_2)_{13}$  supermolecule is  $\text{HI}(\text{H}_2)_{13}$ . The material was synthesized by chemical reaction at pressure inside a diamond anvil cell<sup>14</sup>. The simple-cubic arrangement of the iodine atoms was observed by X-ray diffraction, and the iodane and hydrogen molecules were identified by their characteristic Raman vibron frequencies. The composition was determined by matching the density to the known  $\text{I}_2$  and  $\text{H}_2$  equations of state. The atomic arrangement was deduced from MD simulations, which support free IH and  $\text{H}_2$  rotors at 300 K. Binns *et al.* demonstrated the *average* icosahedral symmetry of the supermolecule by plotting the mean *atomic* positions: for a free-rotating HI molecule, the mean H position is close to the centre of the Iodine while for  $\text{H}_2$  the mean position of both atoms is the same: the molecular centre.

In analogy with other binary  $\text{AB}_{13}$  systems<sup>39–43</sup> two clear candidate structures involving cuboctahedral ( $Pm\bar{3}m$ ) and icosahedral ( $Fm\bar{3}c$ )  $(\text{H}_2)_{13}$  supermolecules emerge. In order to find out the favoured structure, we carried out NPT ab-initio molecular dynamics simulation on these two phases at 30 GPa and 300 K, using the PBE functional. Using a primitive cubic cell, both  $Pm\bar{3}m$  (28 atoms) and  $Fm\bar{3}c$  (56 atoms) remained stable over 3 ps. Using a larger cell with 224 atoms compatible with either structure, simulations started with cuboctahedral supermolecules spontaneously transformed to icosahedral ones. The molecular rearrangement is abrupt, and can be seen in the mean square displacement (MSD) shown in Fig. 2. This proves that the  $Fm\bar{3}c$  structure, with two oppositely aligned icosahedral supermolecules, is the stable structure.

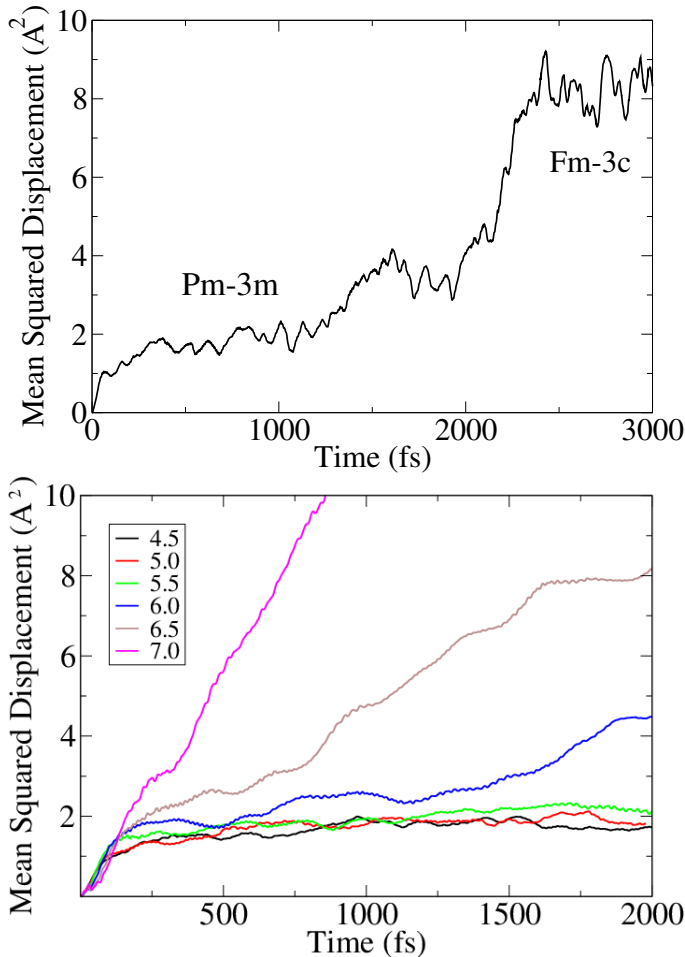


FIG. 2: (*top*) MSD discontinuity at 2200 fs showing transformation of supermolecule in  $\text{HI}(\text{H}_2)_{13}$  from cuboctahedral to icosahedral. (*bottom*) MSD for  $\text{HCl}(\text{H}_2)_{13}$  at 300 K and a range of lattice parameters, in Å, as shown in the legend. The divergent MSDs correspond to low pressures below 7 GPa.

We then examined the possibility of recovering of the supermolecule. This was done using a series of calculations at 300 K the NVT ensemble, using the BLYP functional, and gradually reducing the density. (Results are similar to the  $\text{HCl}(\text{H}_2)_{13}$  data in Fig. 2b, movies are available in SM). At lattice parameters greater than 7 Å, the structure becomes unstable.

We found that  $\text{HI}(\text{H}_2)_{13}$  remains stable in a pressure range between 6–100 GPa. The equation of state is shown in Fig. 3. We used the projection method to calculate the vibrational frequencies of the Raman-active vibrons. This showed that the two hydrogen environments have very similar vibrational frequency, and we were unable to distinguish a doublet. The frequency is significantly different from pure hydrogen at the same pressures. The HI vibron provides a well defined signature for iodane. We also did one run setting the Iodine mass to that of hydrogen: although the dynamics are affected, in classical Born-Oppenheimer MD, the free energy landscape is

mass independent, so this is equivalent to sampling for 200 ps — still no structural transformation occurred.

### B. Predicted compounds: $\text{HBr}(\text{H}_2)_{13}$ , $\text{HCl}(\text{H}_2)_{13}$ and $\text{Xe}(\text{H}_2)_{13}$

Having established that molecular dynamics can determine the stability of the supermolecule phases, we investigate a number of other possible materials based on the same structure. The dynamic nature of the structure means that standard methods of ab initio structure searching for static lattices cannot describe the symmetry. So we resorted again to molecular dynamics, to determine the metastability of the structures.

At higher pressures, all three tested compounds were found to remain stable throughout the simulations (up to 6 ps) at high pressures, but at lower pressures the molecules began to exchange positions within and between icosahedra, effectively forming a solution of HI, HBr or HCl in fluid hydrogen. We believe that the implication is that on longer timescales the compound will be unstable at low density. This is shown by the divergent MSD of the hydrogen atoms in  $\text{HCl}(\text{H}_2)_{13}$  for lattice parameters above 6.0 Å (Fig. 2b). Similar behavior is seen for both BLYP and PBE functionals at the same density.  $\text{HCl}(\text{H}_2)_{13}$  is the most unstable of the materials here: equivalent calculations for  $\text{HI}(\text{H}_2)_{13}$ ,  $\text{HBr}(\text{H}_2)_{13}$ ,  $\text{HI}(\text{H}_2)_{13}$ ,  $\text{Xe}(\text{H}_2)_{13}$  respectively showed the breakdown in stability occurs at increasing volume. The Xe compound did not break down, even at ambient pressure, and appears to be most stable.

Comparative equations of state calculated with BLYP are shown in Fig. 3. The three halide compounds show a clear trend in the lattice parameter, with Xe falling between the HI and HBr compounds. This scaling with molecular size is expected, much more interesting is the comparison of the RDFs.

Comparing different compounds at the same *volume* (Fig. 4), the RDFs of the structures are essentially identical, apart from the halide bondlength. However, because of the different equations of state, for different compounds at the same *pressure*, the supermolecule has very different intermolecular distances. The supermolecule behaviour is primarily determined by the hydrogen density: the halide molecules provide an additional “*chemical pressure*” which determines the total pressure at a given hydrogen density.

The equivalence of the hydrogen structure for all compounds implies that the difference in pressure is mainly attributable to the halide/Xe sublattice. Fig. 4 shows that the larger IH halide compound is associated with the higher pressures. However this “molecular volume” argument is incompatible with the fact that the HI- $\text{H}_2$  intermolecular distances are the same as for HBr- $\text{H}_2$  and HCl- $\text{H}_2$ . Another possibility is that the materials with the higher permanent dipole moment have stronger cohesion, due to dipole-dipole correlations, and hence lower

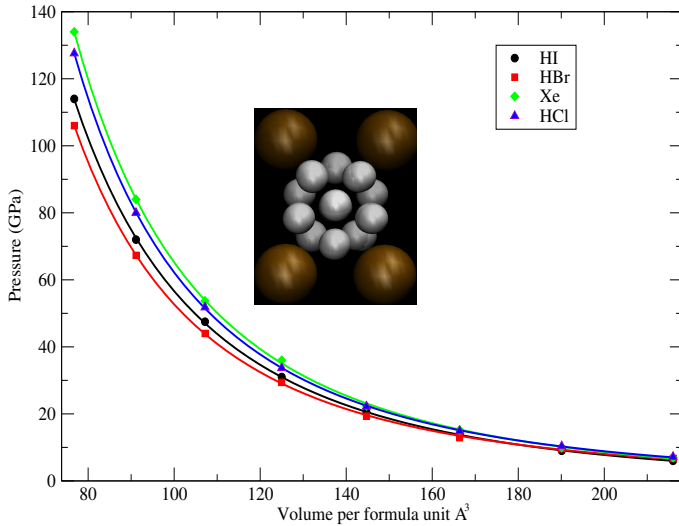


FIG. 3: Equations of state calculated using the BLYP functional. The relative ordering of the curves is independent of the functional, but other functionals tested give lower values of pressure, so the systematic error in the calculated pressure is of order  $\pm 5$  GPa. Symbols are calculated pressure averages with statistical error less than symbol size. Lines show fits to Murnaghan equation of state. Inset show the mean atomic positions for  $\text{IH}(\text{H}_2)_{13}$ , emphasizing the fivefold axis of the supermolecule.

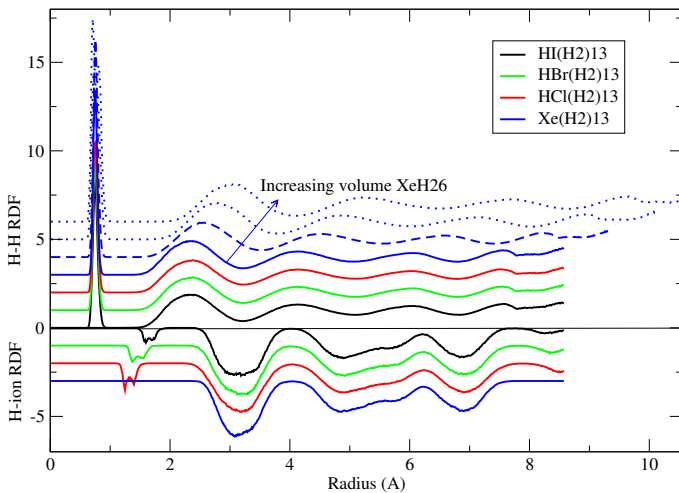


FIG. 4: Radial distribution functions for hydrogen H-H (top) and H-X (bottom,  $X=\text{Cl}, \text{I}, \text{Br}, \text{Xe}$ ) for different compounds at the same lattice parameter ( $5.5\text{\AA}$ ), and for the same compound,  $\text{Xe}(\text{H}_2)_{13}$ , at different densities (top lines in upper panel).

external pressure. This explanation works well for the halides, but is problematic with respect to the Xe compound which has no dipole interactions. Whatever the explanation, it is clear that the pressure at which the supermolecule is stabilized depends strongly on the other species.

### III. LOW TEMPERATURE PHASE TRANSFORMATIONS

Most free-rotor phases undergo a symmetry-breaking phase transformation when intermolecular forces are strong enough to stop the rotation. In our simulations we observed that during cooling to 100 K there is a transformation in the supermolecule to a low temperature structure where the rotation is frozen and the molecules librate rather than rotate. This can be seen in animation (see SM) and in the angular momentum correlation functions: Fig. 5 show the results for  $\text{Xe}(\text{H}_2)_{13}$  which is the most symmetric structure on account of the monatomic Xe.

In the high-T symmetric phase the molecular orientation is disordered and the rotation remains autocorrelated for a picosecond. At lower-T, the libration is shown by the negative region of the ACF, and subsequent oscillation. The short correlation time indicates that the single-molecule libron is not an eigenmode. It is also notable that the correlation time for the 300 K rotor is much reduced by pressure: this will manifest experimentally as a broadening of the roton peak in spectroscopy. By 15 GPa ( $5.5\text{\AA}$ ) the autocorrelation function has a half-life of less than 100 fs, which corresponds to less than a full rotation.

The Xe compound best illustrates the broken symmetry of the supermolecule ( $\text{H}_2)_{13}$ , since Xe is spherical. The inset in Fig. 5 shows a tendency for the molecules to align along the cubic (100) axes. The VACF-calculated Raman vibron spectrum shows two discernible peaks, separated by over 100 wavenumbers, indicating that there are two distinct  $\text{H}_2$  environments, which would be clear experimental signature of the symmetry-breaking on cooling. In the halogen compounds, the symmetry breaking is more complex because of the dipole moment.

There has been some previous experimental and theoretical work on xenon-hydrogen mixtures at lower hydrogen concentrations (90:10 gas mixtures). Somayazulu *et al.*<sup>44,45</sup> found compounds with stoichiometry  $\text{Xe}(\text{H}_2)_7$  or  $\text{Xe}(\text{H}_2)_8$ . From the scattering pattern, they deduced the existence of covalent Xe-Xe dimer bonds. DFT structure search<sup>46</sup> at these compositions found candidate structures, but were unable to find any Xe-Xe bonding and are compared directly with the experimental data. As mentioned in the Methods section, ground-state structure search inevitably produces symmetry-breaking from the orientation of the hydrogen molecules. Given the initial stoichiometries of these works, it is unlikely that the  $\text{Xe}(\text{H}_2)_{13}$  compound could have been found.

### IV. LATTICE DYNAMICS

The Raman-active hydrogen vibron can be calculated from the MD using the projection method<sup>47,48</sup>. Fig 6 shows the data for  $\text{HI}(\text{H}_2)_{13}$ . Only a single peak is evident, showing that the vibration of the central molecule in  $(\text{H}_2)_{13}$  has the same frequency as the others. More-



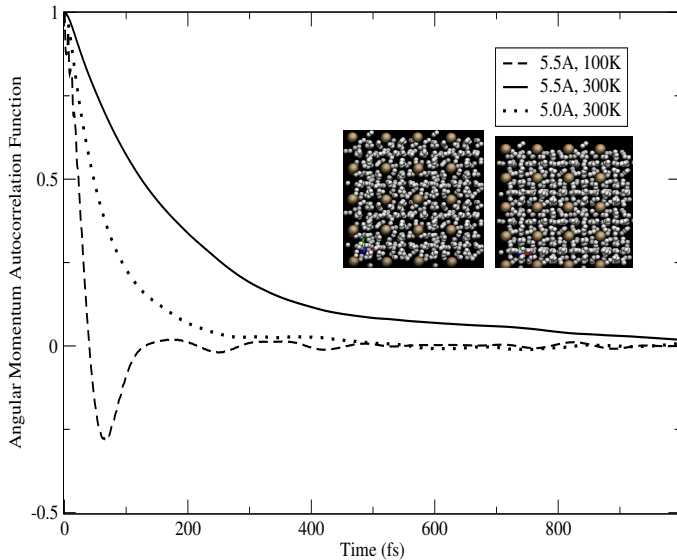


FIG. 5: LACF for  $\text{Xe}(\text{H}_2)_{13}$  at 300 K (continuous) and 100 K (dashed, inset right), with a 5.5 Å lattice parameter. The VACF at 300 K and  $a = 5.0$  Å is shown for comparison. Insets are MD snapshots at 5.5 Å, showing the symmetry-breaking in the hydrogen (small spheres) sublattice on cooling.

over, this frequency is significantly dependent on the functional used. A typical production run of 3 ps allows a discrete Fourier Transform to sample every  $10 \text{ cm}^{-1}$ . This is sufficient to produce a peak around  $4100 \text{ cm}^{-1}$ , but not to discern any trend with pressure, and so all pressures are shown together. Other functionals predict a somewhat lower frequency:  $3920 \text{ cm}^{-1}$  and  $3860 \text{ cm}^{-1}$  for PBE and LDA respectively. Thus despite the structural similarity, there is strong dependence of vibron frequency on functional, correlated with a variation of 2-3% on  $\text{H}_2$  bondlength. Of these, the BLYP frequency is closest to the experimental value:  $4210 \pm 10 \text{ cm}^{-1}$ . A similar calculation for pure hydrogen at 20 GPa produces the red curve in Fig 6, and, despite the noise, it is clear that the hydrogen frequency is tens of wavenumbers higher and probably sharper. The hypothetical compounds mirror this behaviour: the vibron frequency is always lower for the compound than for pure hydrogen. We are not able to discern any trend difference between the compounds, suggesting that the supermolecular environment itself causes the shift.

For classical crystals, Raman intensity calculations using DFT lattice dynamics and perturbation theory are straightforward. However, the small-amplitude approximation breaks down in the limit of freely-rotating molecules: consider for example a molecule pointing along the  $x$  direction, the normal mode corresponding to the stretching mode involves atomic displacements along  $\pm x$ . Suppose that later the molecule rotates to point along the  $y$  direction; now the atomic displacements along  $\pm x$  would correspond to molecular rotation, not stretching. Thus Raman modes cannot be associated

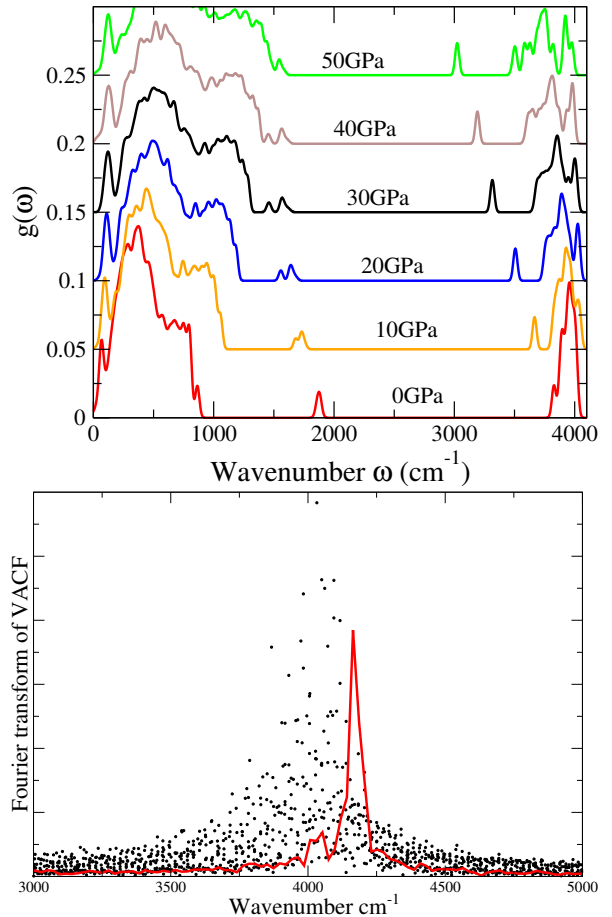


FIG. 6: (*top*) Phonon DoS for a snapshot from  $\text{HI}(\text{H}_2)_{13}$  MD relaxed from 300K at a range of pressures 0, 10, 20, 30, 40, 50GPa. Calculation uses PBE  $3 \times 3 \times 3$  q-point grid and Gaussian broadening with FWHM of  $40 \text{ cm}^{-1}$ : since it is an MD snapshot no attempt is made to interpolate “bands”. (*bottom*) Fourier transform of the VACF projected onto in-phase  $\text{H}_2$  molecular vibrations<sup>35</sup>, for  $\text{HI}(\text{H}_2)_{13}$  (black) and points from discrete Fourier transforms aggregated over all pressures, and a single calculation of pure hydrogen at 20GPa (red).

with cartesian normal-mode eigenvectors. Rotons are not spherical harmonic oscillators, and the quantised energy of a roton is not related to any classical frequency.

Although coupling between rotors and other Raman modes means one cannot simply apply standard lattice dynamics, it is instructive to make some attempt. So we extracted a snapshot from the MD calculation, relaxed it to the nearest zero-temperature enthalpy minimum for a range of pressures, and calculated the phonon density of states (DoS) between 0 and 50 GPa. The results are shown in Fig. 6. Although this is not a definitive representation of the structure, a comparison at different pressures using the same snapshot is meaningful and the Phonon DoS shows a number of interesting features.

Firstly, the main effect of pressure is to broaden the vibron band, and shift it to lower frequencies. Secondly, the mode has much lower frequency than the

equivalent vibron in pure hydrogen (e.g. using identical settings the Raman mode for pure hydrogen<sup>52</sup>, at 30 GPa is 4292  $\text{cm}^{-1}$ ). This is consistent with the observation of Binns et al. who saw two vibrons and attributed the higher frequency mode to pure hydrogen.<sup>14</sup> The  $\text{H}_2$  molecule bondlength is around 0.75 Å, compared to 0.736 Å in pure hydrogen. It suggests that the H-H bond in the supermolecule is weaker, more like that in hydrogen Phase III which occur at much greater pressure.

Our phonon calculation also shows a pronounced weakening of the IH bond with pressure, from 2000 to 1500  $\text{cm}^{-1}$ : again consistent with experiment. The reason for this can also be seen in by a detailed analysis of the modes. One mode in Fig. 6, corresponding to a single  $\text{H}_2$  molecule, becomes detached from the main vibron band and significantly weakens with pressure. Interestingly, the molecule in question is *not* the one in the centre of the supermolecule, rather it is the one closest to the H ion in the IH molecule. By 50 GPa, its bondlength has stretched to 0.843 Å, and the Mulliken bond population is  $\sim 25\%$  lower than other molecules. Even so, this vibron has a much higher frequency than the rotation of the IH molecule. So it is reasonable to treat the IH dipole orientation as fixed throughout many vibrational periods of the vibron: in short, we believe that this bond weakening is real. The weakened  $\text{H}_2$  bond would be difficult to detect by spectroscopy, because with a lifetime equivalent to the rotation rate of the IH, it will have a linewidth of hundreds of wavenumbers, not the arbitrarily-chosen 40  $\text{cm}^{-1}$  of the figure. However, as they rotate, all the IH will *always* have a nearby hydrogen, so the weakening of its bond is permanent and detectable.

Comparing the two phonon methods, we see that the projection method gives a smaller range of vibron frequencies than the lattice dynamics, as expected since they are only the Raman active modes. Using the full VACF without projection gives a broader band and the low frequency modes, similar to the lattice dynamics. VACF also picks out the IH vibron, but not the weakening  $\text{H}_2$  mode: this strongly suggests that the latter mode is an artifact of the snapshot used in the lattice dynamics.

## V. DISCUSSION

We have shown that the icosahedral  $(\text{H}_2)_{13}$  supermolecule is a unit from which to build hydrogen-rich crystal structures. The structure is similar to some  $\text{AB}_{13}$  compounds, such as  $\text{NaZn}_{13}$  and beryllium-rich intermetallics. But whereas those are held together by metallic bonding,  $(\text{H}_2)_{13}$  is unique in having only van der Waals or quadrupole interactions to stabilize it. An alternative reason for stability of  $\text{AB}_{13}$  is observed in binary hard sphere mixtures and opals (packed  $\text{SiO}_2$  spheres) because it has low entropy thanks to its dense packing.<sup>41,43</sup>

The icosahedral, 13-member supermolecule has been calculated to be the most stable molecular cluster dues

to van der Waals interaction in Lennard-Jonesium and in hydrogen<sup>49-51</sup>. The motif cannot be extended to fill homogeneous 3D space, but the current study demonstrates that by packing alongside other molecules, extended structures can be built from this stable cluster.

In DFT calculations, the fundamental quantity is the volume. Pressure is a derived quantity, and the work emphasises the dependence of the pressure on exchange-correlation functional. In particular, the BLYP functional, known to give the closest agreement with Quantum Monte Carlo<sup>24,25</sup> for dense hydrogen, gives calculated pressures higher than other functionals or experiments. The robust conclusions of this paper are therefore framed in terms of density rather than pressure.

The key question for understanding the prospects for recoverability is whether the supermolecule is primarily stabilized by:

- free energy of the hydrogen molecules themselves,
- interactions involving HI, Xe, HBr or HCl molecules,
- the external pressure and efficient packing ( $PV$ ).

In the present cases, the evidence is in favor of packing efficiency: although the HBr, HCl and HI molecule have dipole moments, the structure persists when they are freely rotating, and the Xe compound is unlikely to be stabilised by long - range Xe-Xe bonds. Furthermore, the hydrogen structure is the same in all compounds at the same lattice parameter, while the intermolecular distances within the supermolecule are highly dependent on density. Explicit treatment of van der Waals interactions is critical at low densities in hydrogen, but of secondary importance at pressure<sup>26</sup>. Here van der Waals interactions modelled by the Tkatchenko-Scheffler correction to PBE produced the same structures, further evidence that packing via the  $PV$  term in the enthalpy is more important. There is no characteristic supermolecule size. Nevertheless, the pressure is dependent on the minority species.

The hydrogen molecules in the supermolecule show a number of behaviours typical of pure hydrogen at higher pressures. In all cases the  $\text{H}_2$  bonds are weaker than in pure hydrogen at equivalent pressures; this manifests both as longer bondlengths and lower vibrational frequencies. Also, the supermolecule transforms to a broken-symmetry structure at low temperature and rotation becomes inhibited at higher pressure: features observed in pure hydrogen at higher pressures. Hence it is conceivable that on further pressure increase this supermolecular network might become electrically conducting.

If the molecular-spaced  $\text{H}_{26}$  cannot be recovered, another possible route to hydrogen-storage utilizing  $(\text{H}_2)_{13}$  is a caged structure with cavities tuned to the size of the supermolecule.

Whether recoverable to ambient conditions or not, these supermolecules compounds have novel and exceptional properties: The combination of extreme stoichiom-



etry and incorporation of fivefold symmetry within a crystal structure are properties previously exhibited by fullerene compounds. The icosahedral supermolecule is stable in a range of environments and will be the basis of a new class of ordered hydrogen-rich compounds.

### Acknowledgments

We would like to thank EPSRC for computing resources through the UKCP project, the ERC ‘‘Hecate’’

fellowship for GJA, and the Royal Society Wolfson Award.

- 
- <sup>1</sup> P. Jena, *J. Phys. Chem. Lett* **2**, 206 (2011).  
<sup>2</sup> N. W. Ashcroft, *Physical review letters* **92**, 187002 (2004).  
<sup>3</sup> A. Drozdov, M. Erements, I. Troyan, V. Ksenofontov, and S. Shylin, *Nature* **525**, 73 (2015).  
<sup>4</sup> M. Einaga, M. Sakata, T. Ishikawa, K. Shimizu, M. I. Erements, A. P. Drozdov, I. A. Troyan, N. Hirao, and Y. Ohishi, *Nature physics* **12**, 835 (2016).  
<sup>5</sup> N. W. Ashcroft, *Phys. Rev. Letters* **21**, 1748 (1968).  
<sup>6</sup> C. J. Pickard and R. J. Needs, *Phys. Rev. Letters* **97**, 045504 (2006).  
<sup>7</sup> M. Martinez-Canales, A. R. Oganov, Y. Ma, Y. Yan, A. O. Lyakhov, and A. Bergara, *Physical review letters* **102**, 087005 (2009).  
<sup>8</sup> I. Errea, M. Calandra, C. J. Pickard, J. R. Nelson, R. J. Needs, Y. Li, H. Liu, Y. Zhang, Y. Ma, and F. Mauri, *Nature* **532**, 81 (2016).  
<sup>9</sup> S. Zhang, Y. Wang, J. Zhang, H. Liu, X. Zhong, H.-F. Song, G. Yang, L. Zhang, and Y. Ma, *Scientific reports* **5** (2015).  
<sup>10</sup> G. Zhong, C. Zhang, X. Chen, Y. Li, R. Zhang, and H. Lin, *The Journal of Physical Chemistry C* **116**, 5225 (2012).  
<sup>11</sup> H. Liu, Y. Li, G. Gao, J. S. Tse, and I. I. Naumov, *The Journal of Physical Chemistry C* **120**, 3458 (2016).  
<sup>12</sup> M. Erements, I. Trojan, S. Medvedev, J. Tse, and Y. Yao, *Science* **319**, 1506 (2008).  
<sup>13</sup> I. Errea, M. Calandra, C. J. Pickard, J. Nelson, R. J. Needs, Y. Li, H. Liu, Y. Zhang, Y. Ma, and F. Mauri, *Physical review letters* **114**, 157004 (2015).  
<sup>14</sup> J. Binns, P. Dalladay-Simpson, M. Wang, G. J. Ackland, E. Gregoryanz, and R. T. Howie, *Physical Review B* **97**, 024111 (2018).  
<sup>15</sup> F. Peng, Y. Sun, C. J. Pickard, R. J. Needs, Q. Wu, and Y. Ma, *Physical Review Letters* **119**, 107001 (2017).  
<sup>16</sup> C. J. Pickard and R. Needs, *Journal of Physics: Condensed Matter* **23**, 053201 (2011).  
<sup>17</sup> Y. Wang, J. Lv, L. Zhu, and Y. Ma, *Computer Physics Communications* **183**, 2063 (2012).  
<sup>18</sup> E. Zurek, R. Hoffmann, N. Ashcroft, A. R. Oganov, and A. O. Lyakhov, *Proceedings of the National Academy of Sciences* **106**, 17640 (2009).  
<sup>19</sup> M. Somayazulu, L. Finger, R. Hemley, and H. Mao, *Science* **271**, 1400 (1996).  
<sup>20</sup> J. Binns, X.-D. Liu, P. Dalladay-Simpson, V. Afonina, E. Gregoryanz, and R. T. Howie, *Physical Review B* **96**, 144105 (2017).  
<sup>21</sup> S. J. Clark, M. D. Segall, C. J. Pickard, P. J. Hasnip, M. I. Probert, K. Refson, and M. C. Payne, *Zeitschrift für Kristallographie-Crystalline Materials* **220**, 567 (2005).  
<sup>22</sup> C. Lee, W. Yang, and R. G. Parr, *Physical review B* **37**, 785 (1988).  
<sup>23</sup> A. D. Becke, *Physical review A* **38**, 3098 (1988).  
<sup>24</sup> R. C. Clay III, J. Mcminis, J. M. McMahon, C. Pierleoni, D. M. Ceperley, and M. A. Morales, *Phys. Rev. B* **89**, 184106 (2014).  
<sup>25</sup> S. Azadi and W. M. C. Foulkes, *Phys. Rev. B* **88**, 014115 (2013).  
<sup>26</sup> S. Azadi and G. J. Ackland, *Physical Chemistry Chemical Physics* **19**, 21829 (2017).  
<sup>27</sup> J. P. Perdew, K. Burke, and M. Ernzerhof, *Phys.Rev.Letters* **77**, 3865 (1996).  
<sup>28</sup> J. P. Perdew, A. Ruzsinszky, G. I. Csonka, O. A. Vydrov, G. E. Scuseria, L. A. Constantin, X. Zhou, and K. Burke, *Physical Review Letters* **100**, 136406 (2008).  
<sup>29</sup> J. P. Perdew and A. Zunger, *Physical Review B* **23**, 5048 (1981).  
<sup>30</sup> A. Tkatchenko and M. Scheffler, *Physical review letters* **102**, 073005 (2009).  
<sup>31</sup> G. J. Ackland and I. B. Magdău, *Cogent Physics* **2**, 1049477 (2015).  
<sup>32</sup> S. A. Bonev, E. Schwegler, T. Ogitsu, and G. Galli, *Nature* **431**, 669 (2004).  
<sup>33</sup> H. Liu, L. Zhu, W. Cui, and Y. Ma, *J.Chem.Physics* **137**, 074501 (2012).  
<sup>34</sup> H. Liu, H. Wang, and Y. Ma, *Journal of Physical Chemistry C* **116**, 9221 (2012).  
<sup>35</sup> I. B. Magdău and G. J. Ackland, *Phys. Rev. B* **87**, 174110 (2013).  
<sup>36</sup> I. B. Magdău and G. J. Ackland, *J. Phys.: Conf. Ser.* **500**, 032012 (2014).  
<sup>37</sup> R. T. Howie, I. B. Magdău, A. F. Goncharov, G. J. Ackland, and E. Gregoryanz, *Phys. Rev. Letters* **113**, 175501 (2014).  
<sup>38</sup> I. B. Magdău, M. Marques, B. Borgulya, and G. J. Ackland, *Phys.Rev.B* **95**, 094107 (2017).  
<sup>39</sup> D. P. Shoemaker, R. E. Marsh, F. J. Ewing, and L. Pauling, *Acta Crystallographica* **5**, 637 (1952).  
<sup>40</sup> K. J. Nordell and G. J. Miller, *Inorganic chemistry* **38**, 579 (1999).  
<sup>41</sup> M. Eldridge, P. Madden, and D. Frenkel, *Molecular physics* **79**, 105 (1993).  
<sup>42</sup> A. B. Schofield, P. N. Pusey, and P. Radcliffe, *Physical Review E* **72**, 031407 (2005).  
<sup>43</sup> A. N. Jackson and G. J. Ackland, *Phys. Rev. E* **76**, 066703 (2007).

- <sup>44</sup> M. Somayazulu, P. Dera, A. F. Goncharov, S. A. Gramsch, P. Liermann, W. Yang, Z. Liu, H.-k. Mao, and R. J. Hemley, *Nature chemistry* **2**, 50 (2010).
- <sup>45</sup> M. Somayazulu, P. Dera, J. Smith, and R. J. Hemley, *The Journal of chemical physics* **142**, 104503 (2015).
- <sup>46</sup> T. Kaewmaraya, D. Y. Kim, S. Lebegue, C. J. Pickard, R. J. Needs, and R. Ahuja, *Physical Review B* **84**, 092101 (2011).
- <sup>47</sup> U. Pinsook and G. J. Ackland, *Phys. Rev. B* **59**, 13642 (1999).
- <sup>48</sup> G. Ackland and I. Magdău, *High Pressure Research* **34**, 198 (2014).
- <sup>49</sup> D. J. Wales and J. P. Doye, *The Journal of Physical Chemistry A* **101**, 5111 (1997).
- <sup>50</sup> J. E. Cuervo and P.-N. Roy, *The Journal of chemical physics* **125**, 124314 (2006).
- <sup>51</sup> J. Martínez, M. Isla, and J. Alonso, *The European Physical Journal D* **43**, 61 (2007).
- <sup>52</sup> Using the  $Pca2_1$  structure, a candidate for the ordered hydrogen Phase II.